Lab on a Chip

Accepted Manuscript

ROYAL SOCIETY OF CHEMISTRY

www.rsc.org/loc

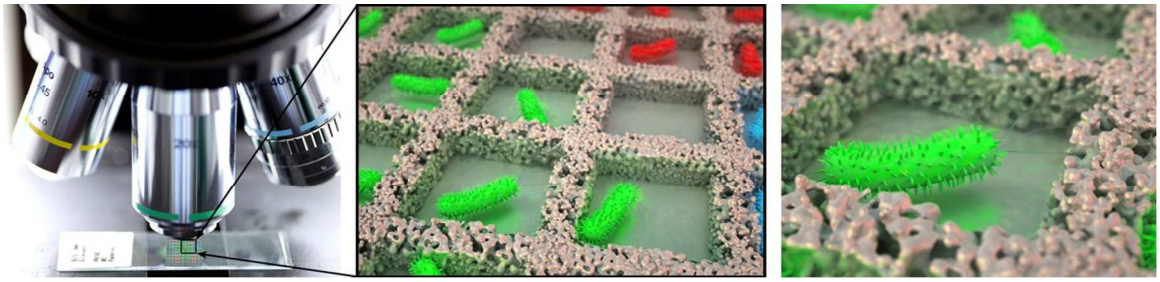

Nanoporous microscale microbial incubators allow communities of microbes to grow in physical isolation while maintaining chemical communication, facilitating the study of interactions within diverse communities

Lab on a Chip

RSCPublishing

ARTICLE

Nanoporous Microscale Microbial Incubators

Cite this: DOI: 10.1039/x0xx00000x

Zhifei Ge[a], Peter R. Girguis[b] and Cullen R. Buie[a]

Received xxth January xxxx,
Accepted xxth January xxxx

DOI: 10.1039/x0xx00000x

www.rsc.org/

Reconstruction of phylogenetic trees based on 16S rRNA gene sequencing reveals abundant microbial diversity that has not been cultured in lab. Many attribute this so-called 'great plate count anomaly' to traditional microbial cultivation techniques, which largely facilitate growth of a single species. Yet, it is widely recognized that bacteria in nature exist in complex communities. One technique to increase the pool of cultivated bacterial species is to co-culture multiple species in a simulated natural environment. Here we present nanoporous microscale microbial incubators (NMMI) that enable high-throughput screening and real-time observation of multi-species co-culture. The key innovation in NMMI is that they facilitate inter-species communication while maintaining physical isolation between species, which is ideal for genomic analysis. Co-culture of a quorum sensing pair demonstrates that the NMMI can be used to culture multiple species in chemical communication while monitoring growth dynamics of individual species.

Introduction

16S ribosomal RNA gene sequencing has been used to identify and classify bacteria [1-2] and have revealed abundant microbial diversity in nature. It is estimated that the number of bacterial species is about 2 x 10^6 in sea and 4 x 10^6 in soil [3]. However, the number of cultivated bacterial species listed in DSMZ (German Collection of Microorganisms and Cell Cultures GmbH), one of the largest biological resource centres worldwide, is just above 11,500 as of January 2015 [4]. Thus, the number cultivated bacterial species is several orders of magnitude lower than the estimated number of species in nature. This significant difference has been noted as the great plate count anomaly [5]. Several methods have been pursued to increase the number of cultivated species including optimization of both enrichment [6-12] and cultivation techniques [13-19].

Among all the efforts to increase the pool of cultivated species, Lewis and co-workers [20-21] pioneered cultivating environmental samples in simulated natural environments while physically isolating each bacterial species. In such environments, multiple bacterial species are co-cultured in diffusion chambers with porous walls. The diffusion chamber walls contain pores that are small enough to physically isolate cells while large enough to allow diffusion of metabolites secreted by the organisms. Different species can be cultured in different diffusion chambers, while all chambers can be incubated in a common aqueous environment. In this way, cross-feeding between species is retained while competition among species is suppressed. An optimized spatial structure has been demonstrated to stabilize synthetic multi-species bacterial communities [22].

Since then, the concept of cell compartmentalization with diffusion chambers has been further explored by other researchers. In the earliest proof-of-concept work, Lewis and co-workers [20] sandwiched washers with 0.03-μm pore polycarbonate membranes to build diffusion chambers. However, this method has limited throughput. Miniaturized diffusion chambers, called Ichip[21], for parallel cultivation and isolation have been developed by Nichols and co-workers to increase throughput. Later work using the Ichip has shown that the device be used to study uncultured bacteria of their ability to produce antibiotics[23]. Zengler and co-workers [24] increased the throughput by encapsulating cells in gel microdroplets, and culturing all gel microdroplets massively in parallel under low nutrient flux. Using electrical signal to electrodeposit hydrogel, Cheng and co-workers are able to control population density and distribution[25]. Ingham and co-workers [26] designed a high throughput million-well growth chip with discrete compartments as small as 7 x 7 μm to recover uncultivated bacterial species. During cell culture, the million-well growth chip floats on culture media for nutrient supply. Ma and co-workers [27] combine microbial genetics and compartmentalized miniature cell culture for genetically targeted cultivation of microorganisms. They designed a workflow that integrates stochastic confinement in microfluidic chambers and individual addressable replica microbial cultures known as SlipChip [28]. Notably, Ma and co-workers were able to recover a microorganism from the Human Microbiome Project's "Most Wanted" list [27].

However, none of the devices mentioned enable studies of growth dynamics in real time without compromising throughput, which is key to understanding the complex systems biology of microbial communities. As a potential solution this paper presents nanoporous microscale microbial incubators (NMMI) that enable high-throughput screening and real-time observation of multi-species co-culture. The key innovation in the NMMI is the combination of high throughput screening, physical species isolation, and inter-species communication, all on a single device. The NMMI is a useful platform for the investigation of inter-species chemical communication. When the nature of inter-species chemical communication is unknown, such as in an environmental sample, the NMMI can be used to recover clusters of microbes that are cultured in isolated chambers. Cells recovered from NMMI can subsequently be sequenced to obtain the genomic profile of the recovered samples. Sequencing clusters of cells recovered from the NMMI can be much less expensive than sequencing

environmental cells directly since each chamber would contain cells with a common ancestor. The NMMI system facilitates screening a community for the syntrophic interactions that lead to cell growth. Once potentially interacting organisms are identified via sequencing they can be removed from the system for cultivation in another device that can screen for metabolites.[42] Secondly, the NMMI can be used to quantitatively study known inter-species chemical communication. It has been shown in simulations using game theory that diffusivity of public goods influences microbial mutualism [43]. It is easy to modulate chemical transport between microbes in the NMMI by altering the porosity and thickness of the materials used. Efficacy of the NMMI is demonstrated on a pair of engineered quorum sensing organisms, highlighting the benefits of isolating organisms physically while facilitating chemical communication.

Materials and Methods

Device design and fabrication

Nanoporous hydrogels are used to create micro-well arrays on transparent glass slides. Each well is a diffusion chamber to facilitate physically isolated cell culture while allowing chemical diffusion. As shown conceptually in fig. 1, when seeded in the ideal case, each species of bacteria occupies a single well and grows within the well. Bacteria cannot cross the nanoporous walls while metabolites and other compounds secreted by the bacteria can.

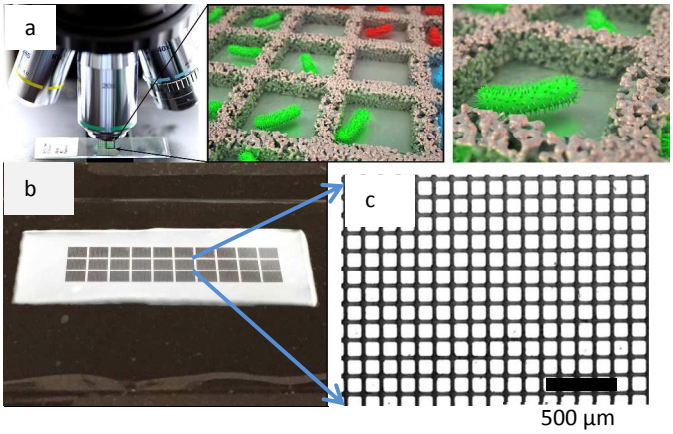

Fig. 1 Schematic and digital images of the nanoporous microscale microbial incubators (NMMI). a) Working principle of the NMMI device. Individual cells are stochastically seeded into individual incubators such that there is one cell per chamber on average. The wall of the chamber is nanoporous. Pores are small enough to physically isolate cells, though large enough to allow diffusion of metabolites and other compounds secreted by cells. b) Digital image of the fabricated NMMI. c) Magnified view of the NMMI with optical microscope. The scale bar is 500 µm.

The nanoporous walls are fabricated with replica molding of soft lithography[29], a process that is easily scalable. With soft lithography, resolution of 10 µm features are easily obtained, ideal for the present application to microbial cultivation. In this work each chamber has dimensions of 100 µm x 100 µm x 100 µm with 25 µm thick walls, thus 10,000 wells can occupy an area less than three square centimeters.

The NMMI is fabricated as shown in Fig. 2. In steps 1 and 2, an SU-8 (SU-8 2050, Microchem, Newton, MA, USA) master mold is patterned using photolithography on silicon wafer. The thickness of the SU-8 master mold is about 100 µm. In steps 3 and 4, polydimethylsiloxine (PDMS) (Sylgard 184, Ellsworth, Germantown, WI, USA) is cast onto the SU-8 master mold and cured at 80ºC overnight. The PDMS, once removed from the SU-8 master mold, is used to mold the UV-curable hydrogel of poly(2-hydroxyethyl methacrylateco-ethylene dimethacrylate) (HEMA-EDMA). Before being cured, the nanoporous HEMA-EDMA precursor solution is in liquid phase and readily wets the PDMS mold. The detailed composition of the nanoporous HEMA-EDMA precursor solution is described in the following section. In Steps 5 and 6, the nanoporous HEMA-EDMA precursor solution fills the space between the PDMS mold and the glass slide. The entire sandwiched structure is exposed for 15 min under a UV lamp (Spectroline EA-160, Fisher Scientific, Waltham, MA, USA). After exposure to UV light, the PDMS mold is peeled off the glass slide. The glass slide with cured hydrogel on top is washed with methanol and stored in methanol before use. Storage in methanol is necessary to remove any uncured hydrogel precursor solution or solvent in the fabricated NMMI. Steps 7 and 8 are the cell seeding and encapsulation processes, which is described in detail in a subsequent sections.

The hydrogel does not naturally bond to the surface of the glass surface covalently. Thus, during the shrinking and swelling associated with hydration, HEMA-EDMA can easily detach from the glass surface. The glass surface is first treated with 3-(trimethoxysilyl)propyl methacrylate (Sigma Aldrich, St. Louis, WO, USA) to modify glass surfaces with methacrylate groups in

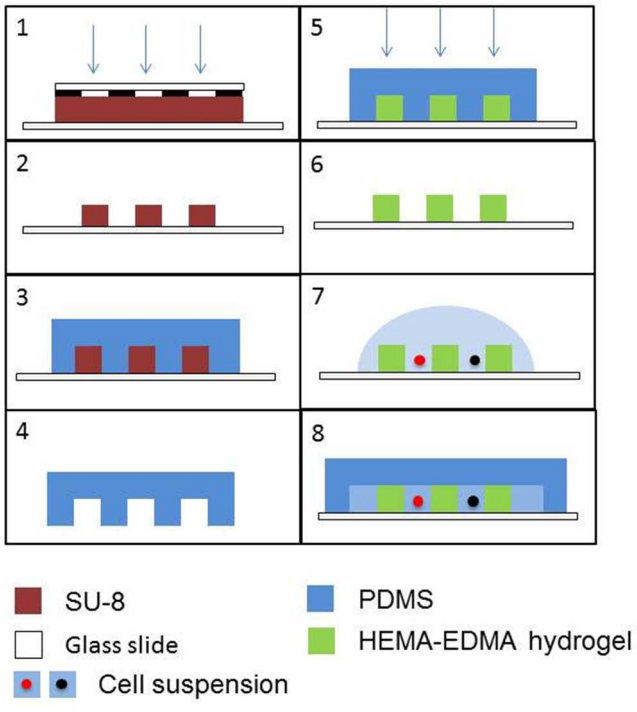

Fig. 2 Schematic illustration of the NMMI fabrication process. 1) Standard photolithography of SU-8. 2) Resulting SU-8 master mold. 3) Casting PDMS to the SU-8 master mold. 4) Resulting PDMS mold. 5) PDMS mold is used to pattern HEMA-EDMA hydrogel. 6) Fabricated NMMI as micro-well arrays of HEMA-EDMA on a glass slide. 7) Statistically seeding of cells into the NMMI by pipetting cell suspension drop on the NMMI. 8) Capping the NMMI with a PDMS cap.

order to covalently attach HEMA-EDMA to the glass surface. Methacrylate groups can be covalently bonded with HEMA-EDMA, if HEMA-EDMA is photo-cross-linked on top of the treated glass slide.

HEMA-EDMA synthesis

In this work, HEMA-EDMA hydrogels are used to create porous structures. The precursor solution contains the monomer, cross-linker and solvent necessary to synthesize the hydrogel. The volume and composition of solvent in the precursor solution influences the structure of the synthesized hydrogel, thus affecting the porosity and average pore size of the hydrogel. The precursor solution is mixed according to a method described elsewhere [30].

The precursor solution to synthesize nanoporous HEMA-EDMA is mixed in the following composition: 2-hydroxyethyl methacrylate (HEMA, Sigma Aldrich) (~24 %wt.), ethylene dimethacrylate (EDMA, Sigma Aldrich) (~16 %wt.), 1-decanol (Sigma Aldrich) (~12 %wt.), cyclohexanol (Sigma Aldrich) (~48 %wt.) and 2,2-dimethoxy-2-phenylacetophenone (Sigma Aldrich) (DMPAP) (~1 %wt with respect to monomers).

The precursor solution to synthesize microporous HEMA-EDMA is mixed in the following composition: 2-hydroxyethyl methacrylate (HEMA) (~24 %wt.), ethylene dimethacrylate (EDMA) (~16 %wt.), 1-decanol (~40 %wt.), cyclohexanol (~20 %wt.) and 2,2-dimethoxy-2-phenylacetophenone (DMPAP) (~1 %wt with respect to monomers).

HEMA-EDMA is cross-linked with UV illumination and in the precursor solution HEMA and EDMA are the monomers. DMPAP is the photo-initiator, while 1-decanol and cyclohexanol is the solvent. It has been shown that changing the ratio of 1-dcanol and cyclohexanol leads to different average pore sizes in the hydrogel [30]. In this work both nanoporous and microporous membranes have been fabricated. A dual chamber diffusion cell was utilized to measure diffusivity of molecules of different sizes through the membranes. The data, discussed below, indicates that membrane pore size can be modulated to allow or suppress transport of molecules of different sizes.

Diffusivity measurement of HEMA-EDMA membrane

A customized dual chamber diffusion cell is employed to measure diffusivity of two representative molecules, glycine (Sigma Aldrich) and bovine serum albumin (BSA) (Sigma Aldrich), across the nanoporous and the microporous hydrogel membranes.

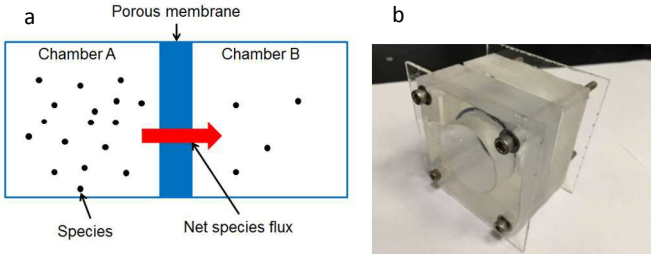

Fig. 3 Dual chamber diffusion cell for diffusivity measurements. A porous membrane (HEMA-EDMA) identical to the walls of the NMMI separates the two chambers. (a) In chamber A, solute of a known certain concentration is seeded, while DI water is added into Chamber B. Over time, the solute diffuse from Chamber A to Chamber B. Measurement of the concentration of the solute in Chamber B over time can be used to derive the diffusivity of the solute across the membrane. (b) Digital image of the dual chamber diffusion cell used in this study. The size of each cylindrical diffusion chamber is 38.1 mm (=1.5 inch) in diameter and 25.4 mm (=1 inch) in height.

The design principle of the dual chamber diffusion cell is shown in Fig. 3. Dilute solution of a particular molecule is seeded in Chamber A with deionized water in Chamber B. If the membrane is permeable to the molecule, the molecule will diffuse across the membrane and the concentration in Chamber B will increase. The actual design of the diffusion cell is shown in Fig. 3b. The cell is built with acrylic plates. The membrane is inserted between the two chambers, and before the two components are linked and tightened with bolts and nuts.

According to the transport theory of dilute solutions, the concentration of molecules in chamber B follows a time-dependent diffusion model [31]:

$$-\ln\left(1-\frac{C_B(t)}{C_\infty}\right)=\frac{D}{h}\left(\frac{t}{\tau}\right) \quad (1)$$

Where $C_B(t)$ is the chemical concentration in Chamber B; C_∞ is the steady state chemical concentration in chamber B, and in the case of equal chamber sizes, C_∞ is half the initially seeded concentration of the molecule in Chamber A. D is the effective diffusivity; h is the membrane thickness; t is time; V is total volume of the system, including the two chambers and the membrane;

$$V = V_1 + Ah + V_2 \quad (2)$$

V_1 and V_2 are the volumes of the two chambers. A is the area over which diffusion occurs.

τ is a geometric parameter specified by the following expressions [31]:

$$\tau = \frac{(V_1 + Ah/2)(V_2 + Ah/2)}{AV} \quad (3)$$

The solution in chamber B is constantly sampled, and its UV spectrum is measured using a UV/Vis spectrophotometer (UV-1800, Shimadzu Scientific Instruments, Inc.). According to the Beer-Lambert law, chemical concentration of the solution is linearly related to UV adsorption.

$$S(t) = \varepsilon l C_B(t) \quad (4)$$

Where, $S(t)$ is UV absorption measured by the UV/Vis spectrophotometer; ε is molar absorptivity; and l is the pathlength through the sample. When the solute concentration is dilute, ε and l are both constants. Thus, absorption $S(t)$ will be linear with respect to chemical concentration $C_B(t)$. Thus, the time dependent chemical concentration in Chamber B can be obtained by measuring the UV absorption of the solution. The concentration curve can then be fit with the time-dependent diffusion model to derive the diffusivity across the HEMA-EDMA membrane.

Single strain cell culture and seeding

Culture of a single strain is conducted to demonstrate the ability of NMMI to physically isolate cells during cultivation. Here, we use *Escherichia coli* K12 wild type (Yale Coli Genetic Storage Center CGSC4404) transformed to express green fluorescent protein (GFP) constitutively. *E. coli* K12 is transformed with a green fluorescent protein (GFP) expressing plasmid (Parts Registry K176011) by electroporation. The transformed *E. coli* is cultured in Lysogeny broth (LB) media (BD, Franklin Lakes, NJ, USA) containing 50 μg/mL of ampicillin (Sigma Aldrich) at 37ºC with 250 rpm shaking. *E. coli* are stochastically seeded into the NMMI as shown schematically in Fig. 2 Steps 7 and 8. Before the protocol is started, *E. coli* is cultured to stationary phase and then diluted to about 1 million cells per milliliter.

In the cell seeding protocol, a cell suspension drop of about 20 μL is pipetted on top of the HEMA-EDMA micro-well arrays. After 3 minutes, a PDMS cap is applied to seal the system. PDMS is used

because it is permeable to many gases, including oxygen. The depth of the groove in the PDMS cap is made the same as the height of the micro-well arrays. The hydrogel of HEMA-EDMA swells when it absorbs water, therefore although there are no covalent bonds between HEMA-EDMA and PDMS, swelling leads to a compressive force between the cap and the HEMA-EDMA micro-well arrays and contributes to a secure seal.

Construction and culture of *E. coli* quorum sensing (QS) pair

An *E. coli* quorum sensing [32-33, 41] pair was constructed and co-cultured in the NMMI to demonstrate cultivation with inter-species chemical communication and physical isolation. The quorum sensing pair of *E. coli* consists of a sender strain and a receiver strain. The sender strain expresses and secretes signalling molecules at high population density, and the receiver strain can sense the signalling molecules. Here, we construct the sender strain by transforming *E.coli* K12 wild type to express a QS molecule (N-Acyl homoserine lactone, AHL, molecular weight 213.23 g/mol), and construct the receiver strain by transforming *E. coli* K12 wild type with AHL receiver plasmids (Parts Registry T9002). The sender strain is further transformed to express red fluorescent proteins (RFP) constitutively (Parts Registry I13521). Thus, the sender strain can be detected with red fluorescence throughout the culturing process, while the receiver strain will express GFP upon sensing AHL, and can be distinguished from the sender strain with green fluorescence.

The sender strain and the receiver strain are separately cultured in EZ rich defined media (Teknova, Hollister, CA, USA) containing 50 μg/mL of ampicillin at 37ºC with 250 rpm shaking. EZ rich defined media is chosen, instead of LB media, to minimize leaky expression of GFP in the receiver cells. After overnight culture, the cells are diluted 100 times in fresh EZ rich defined media and cultured to exponential phase (OD_{600} between 0.6-0.8). Then, the exponential-phase cell suspensions are diluted to about 10^6 cells/mL with fresh EZ rich defined media. Finally, suspensions of the sender strain and receiver strain are mixed and seeded into the NMMI following the same cell seeding protocol described in the single strain cell culture and seeding section.

Results and Discussions

Microscopic imaging of the hydrogel

The structure of the HEMA-EDMA hydrogel is imaged under a Helium Ion Microscope (Carl Zeiss AG, Germany). To facilitate handling the hydrogel, HEMA-EDMA is synthesized with a glass fiber membrane (47 mm diameter, Pall Corporation), as the scaffold. The as-prepared membrane is kept in the vacuum chamber overnight to eliminate leftover solvent and other volatile compounds, including 1-decanol and cyclohexanol. A 1.5-nm thick layer of gold is sputtered on the hydrogel membrane to facilitate high resolution imaging.

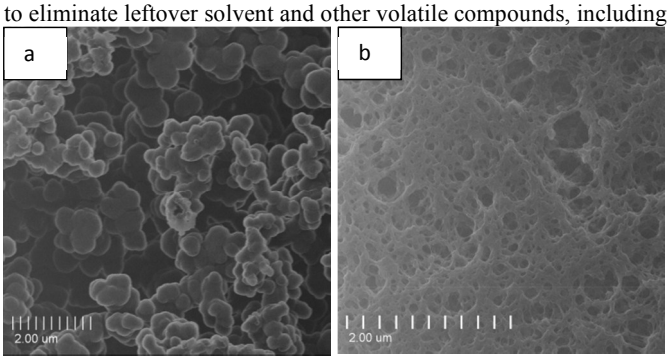

Fig. 4 Helium Ion Microscope (HIM) images of a microporous (a) and a nanoporous (b) HEMA-EDMA membrane. Scale bars in both images are 2 μm.

HIM images of the microporous and nanoporous HEMA-EDMA are shown in Fig. 4 with scale bars of 2 μm. Fig. 4a indicates that the pore size of the nanoporous HEMA-EDMA is less than 200 nm, which is of similar pore size to the 0.2 μm membranes used for cell filtration. Therefore, the nanoporous HEMA-EDMA is very promising for physically isolating bacteria. On the other hand, Fig. 4b indicates that many pores of the microporous HEMA-EDMA are greater than 200 nm and thus insufficient for physical confinement of bacteria. Cell culture experiments (data not shown) confirm that microporous HEMA-EDMA indeed cannot physically isolate bacteria.

The dual chamber diffusion cell for measuring diffusivity across the membrane is used to culture GFP expressing *E. coli* and confirm efficacy in isolating *E. coli*. GFP expressing *E. coli* is seeded into one of the two chambers and cultured overnight in LB media. Cell suspensions in each chamber were sampled the next day and observed under fluorescence microscope. It is observed that with the nanoporous membrane, *E. coli* remain only in the chamber where they were initially seeded, while with the microporous membrane, green fluorescent *E. coli* were observed in both chambers. Therefore, to culture bacteria with physical isolation, the nanoporous HEMA-EDMA is selected. It should be pointed that that pore size and porosity of the HEMA-EDMA can be further optimized by modulating the chemical composition in the precursor solution.

Transport properties of the HEMA-EDMA membrane

Two representative molecules—glycine and bovine serum albumin (BSA)—have been measured for their diffusivity across the nanoporous and microporous membranes using the dual chamber diffusion cell. Glycine, with its molecular formula as NH_2CH_2COOH, has a molecular weight of 75 Da. In contrast, BSA, a serum albumin protein derived from cows, has a molecular weight of ~66 kDa, almost one thousand times larger than glycine. These two molecules are selected to test the permeability of the HEMA-EDMA membranes for molecules of different sizes.

The reference curve for the chemical concentration-UV absorption correlation is obtained by measuring the UV absorption of the solution at known solute concentrations. Fig. 5a provides the correlation for glycine concentration with UV adsorption at 200 nm. Every point in the figure is an average of four measurements with standard deviations indicated. Fig. 5b provides the correlation of BSA concentration with UV adsorption at 280 nm. Different wavelengths of UV light are utilized for each molecule to maximize adsorption. For both glycine and BSA within the range tested, the UV absorption and molecular concentration follow a linear relationship. Fitting with the Beer-Lambert law gives the dependence of UV adsorption on molecular concentration. The constant to relate glycine concentration and OD200 is 0.830 g/L, and the constant to relate BSA concentration and OD280 is 1.580 g/L.

With the reference curve to relate molecule concentration and UV absorption, diffusivity of the molecule across the microporous and the nanoporous membranes can be determined. Chambers A and B are 38.1 mm (=1.5 inch) in diameter with height of 25.4 mm (=1 inch). The thicknesses of the nanoporous and microporous membranes are measured with a calliper and range from 0.40 mm to 0.66 mm. 28 mL of 1.5 g/L (0.02 M) glycine is seeded into Chamber A and 28 mL of DI water in Chamber B. For BSA, the initial concentration in Chamber A is 2 g/L. 150 μL of solution from chamber B is sampled and its UV adsorption is measured every 30 min. The 150 μL solution is returned to the chamber immediately

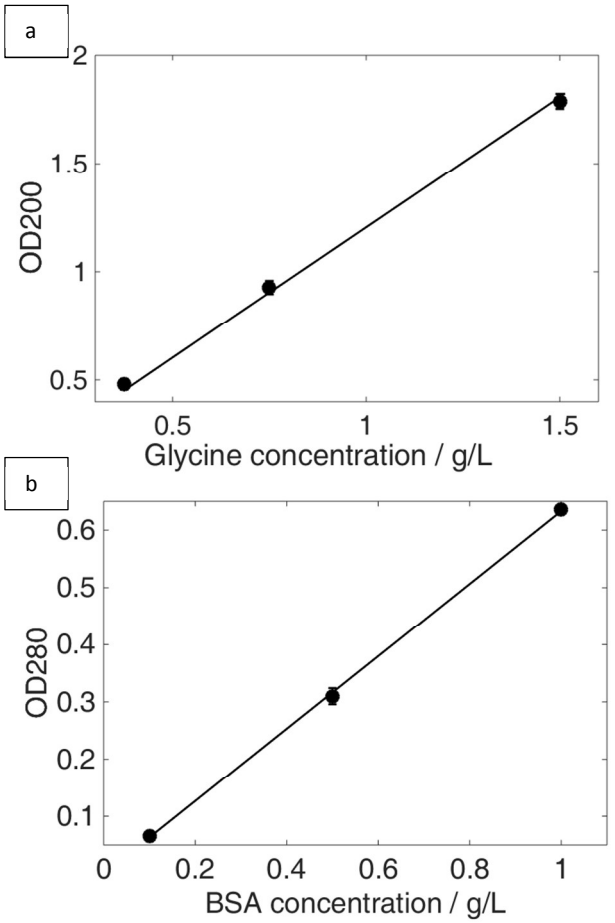

Fig. 5 Reference curve to relate molecule concentration and optical density. In both plots, the symbol ● represents average absorption of four experiments with standard deviation indicated. The solid line curve is the fit results. Slope for relating glycine concentration to OD200 is 0.830 g/L. Slope for relating BSA concentration to OD280 is 1.580 g/L.

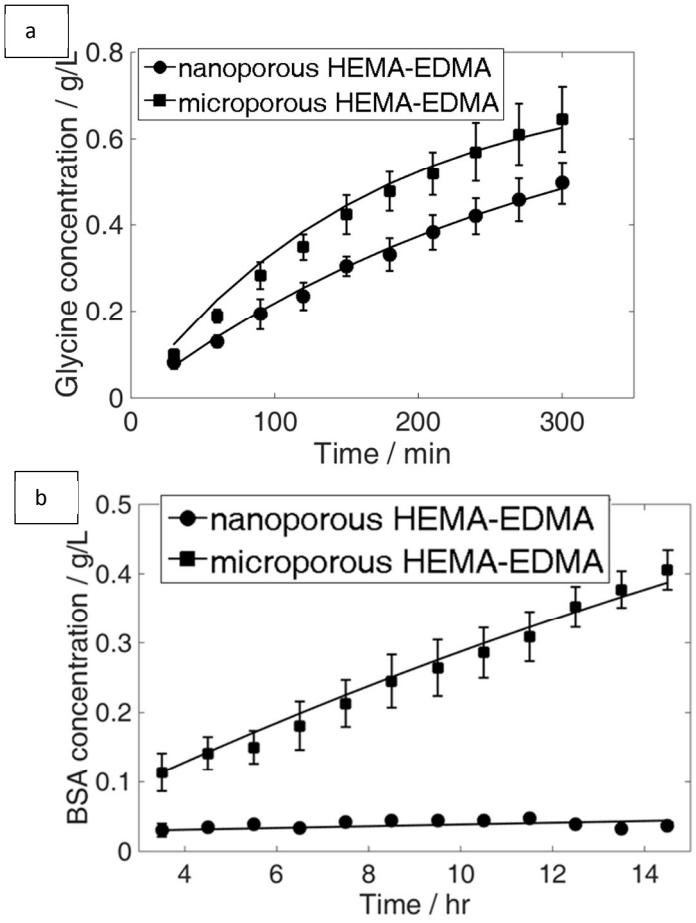

Fig. 6 Time lapse measurement of glycine and bovine serum albumin (BSA) concentration to derive diffusivity. In both plots, the symbols represent the average of four experiments of either glycine or BSA in Chamber B with standard deviation indicated for microporous membranes (squares) or the nanoporous membranes (circles). For the nanoporous membrane, glycine diffusivity is determined to be 3.47 x 10^{-10} m^2/s, and BSA is ~ 0 m^2/s. For the microporous membrane, glycine diffusivity is 6.03 x 10^{-10} m^2/s, and BSA is 1.42 x 10^{-10} m^2/s.

after measurement (More details in the experimental procedure of diffusivity measurement are provided in the Supplementary Information). The concentration for each measurement is calculated using the reference curve. The time dependent chemical concentration plot is fitted with Equation (1), and shown in Fig. 6 as solid lines for both the nanoporous and the microporous membranes.

For the nanoporous membrane, the fitting result gives an effective diffusivity of glycine across the nanoporous HEMA-EDMA membrane as 3.47x10^{-10} m^2/s, and ~0 m^2/s for BSA (Note: because of the thickness of the HEMA-EDMA membrane and time duration of the measurement, diffusivities less than 10^{-12} m^2/s cannot be measured accurately, and is thus approximated here as close to 0).

For the microporous membrane, the fitting result gives an effective glycine diffusivity across the microporous HEMA-EDMA membrane as 6.03 x 10^{-10} m^2/s, and BSA diffusivity of 1.42 x 10^{-10} m^2/s. The glycine is permeable to both the nanoporous and microporous membranes and diffusivity of glycine through the nanoporous membrane is about 58% of that through the microporous membrane. However, BSA is almost non-permeable through the nanoporous membrane, while remaining permeable through the microporous membrane. This is further evidence that the pore sizes of the nanoporous and microporous membranes are very different, which is consistent with the HIM imaging.

Single strain cell culture in the NMMI

In this section, a strain of green fluorescent *E. coli* is seeded into the NMMI, and its growth is monitored with fluorescence microscopy. The purpose of single-strain cell culture is to validate that the NMMI is capable of physically isolating bacteria, and that the HEMA-EDMA is biocompatible.

Physical isolation of cells is recorded by monitoring swimming of an individual cell in a chamber as shown in video S1. In video S1, the microbe is swimming inside the chamber, moving back and forth within the area encompassed by the nanoporous HEMA-EDMA walls. This provides further qualitative evidence that the hydrogel is capable of physically isolating bacteria.

Fig. 7 provides two images of the single-strain *E. coli* culturing in the NMMI. The two images are taken immediately after bacteria are seeded (Fig. 7a), and after 12 hours (Fig. 7b). In Fig. 7a, stochastic distribution of bacteria among the chambers is observed. The number of bacteria inside a chamber ranges from zero to six in this image. The results after 12 hours of culture show that the growth of *E. coli* is highly heterogeneous. Moreover, there are still chambers

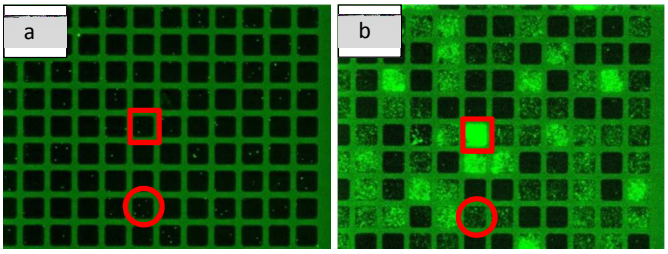

Fig. 7 Growth of *E.* coli with constitutive green fluorescent protein (GFP) expression NMMI. a) Images taken immediately after cells were stochastically seeded into the NMMI. b) Images taken after 12 hours of incubation at room temperature. Growth of *E. coli* is heterogeneous and can be detected by green fluorescence microscopy. The red rectangle and red circle identify two distinct chambers. In these two chambers, more cells were initially seeded in the chamber indicated with the circle than the chamber indicated by the rectangle marked. However, after 12 hours of incubation, cell density in the chamber indicated with the rectangle exceeds that in the chamber marked with the circle.

that are unoccupied by bacteria after many generations of growth. These results show that bacteria cannot migrate between chambers, because if they could the culture results would be more homogeneous.

Comparing Fig. 7a and Fig. 7b, we see that the final growth results are not simply a function of the initial bacterial concentration. In the initial seeding image of Fig. 7a, the chamber marked with a circle (second row from the bottom, sixth column from the left) is the highest bacterial concentration among all chambers in the field of view. The chamber marked with a rectangle (sixth row from the bottom, sixth from the left) contains only two bacteria. However, after 12 hours of culture, fluorescent intensity in the 'rectangle' chamber is significantly higher than that in the 'circle' chamber. It should be pointed out that fluorescence intensity of individual cells varies significantly. Thus, higher fluorescence intensity does not necessarily indicate higher population. However, in Fig. 7b, it is clear that bacteria have filled almost the whole space of the 'rectangle' chamber, while bacteria in the 'circle' chamber remain sparse. This demonstrates that bacterial concentration in the 'circle' chamber is lower than that in the rectangular chamber. There are several reasons that such results are to be expected. For example, the cells initially seeded in the 'circle' chamber may contain a high proportion of dead organisms.

Co-Culture of QS pair in the NMMI

Co-culture of the QS pair is conducted to demonstrate that the NMMI can be used to physically isolate cells and retain inter-species chemical communication. Here, chemical communication is achieved through the QS signalling molecule AHL. To demonstrate inter-species chemical communication between cells occupying different chambers, cells are stochastically seeded into the NMMI at the concentration of about 10^6 cells/mL, and then fluorescence images are taken after overnight culture.

Control experiments are performed to quantitatively demonstrate the significant difference in green fluorescence for receiver cells with and without sender cells in the NMMI. In Fig. 8, we average the green fluorescence in wells with significant growth of receiver cells. The wells that are averaged are marked with white rectangles in Fig. 8a and b. Fig. 8c shows that average green fluorescence in the NMMI is at least an order of magnitude higher for receiver cells cultured in the presence of sender cells than those without. It should also be noted that in Fig. 8a, there is the lower right chamber that

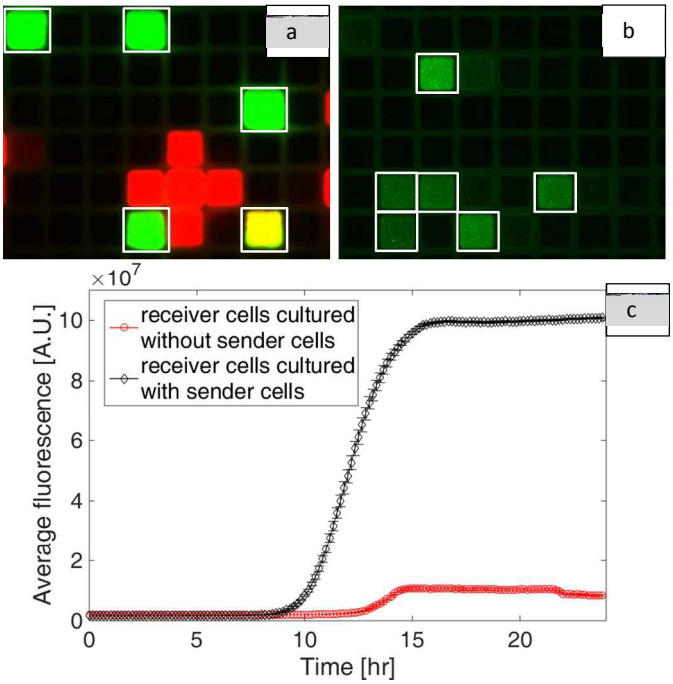

Figure 8. Receiver cells cultured with the presence of sender cells (a) show one order of magnitude higher fluorescence intensity than those without (b). The wells, highlighted with white boxes, are averaged for their green fluorescence in a) and b). Note that in (a) the lower right chamber contains significant growth of both red fluorescent and green fluorescent cells. The average green fluorescence in this chamber is not significantly different from that of other chambers in (a), which is reflected in the small standard deviation in (c). For both experiments, cells are cultured for 24 hours, and the NMMI are mounted on the same position on the microscope, and green fluorescence images are taken every 10 min with 500 ms exposure time.

contains significant growth of both green and red fluorescent cells. Growth of both types of cells in the same chamber is a result of the stochastic seeding process. Clearly from Fig. 8c, the average fluorescence intensity in the lower right chamber is not significantly different than that of other green fluorescent chambers in Fig. 8a. This is further proof that AHL molecules are activating GFP expression in all green fluorescent chambers in Fig. 8a.

Further results from imaging growth dynamics are shown in Fig. 9. Fig. 9a is the image taken immediately after seeding of QS cells. In this image, only red fluorescent cells are observed, which are marked with red circles. This is expected since the receiver cells should not have detected any AHL at such low cell concentrations. After ~16 hours of incubation, as shown in Fig. 8b, we observe physically segregated green fluorescent cells and red fluorescent cells, confirming that AHL molecules diffuse from the red-fluorescent sender cell to the receiver cell to activate GFP expression in the latter. Fig. 8c is a magnified view of the co-culture results. Walls of several chambers are observed to be fluorescent in Fig. 8c, which is likely the result of light reflection or camera saturation. Fig. 8d shows an area where only green fluorescence is observed and no red fluorescence cells are found. In this case, the AHL molecule activating GFP expression must have diffused from wells outside the field of view. This is further proof that the NMMI device is capable of allowing inter-species chemical communication between physically isolated organisms.

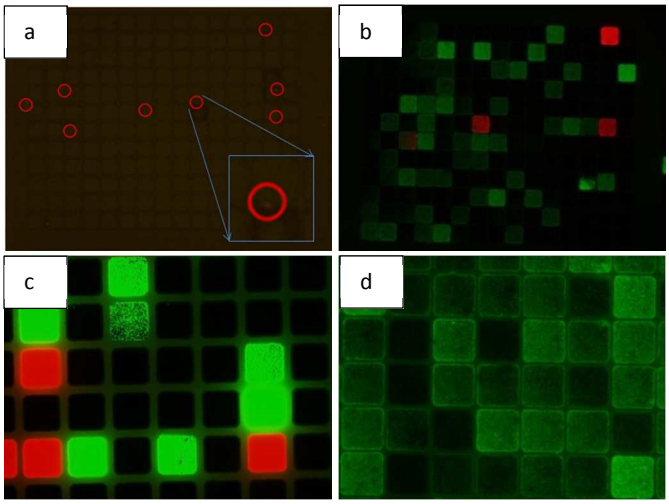

Fig. 9 Co-culture of an *E. coli* quorum sensing (QS) pair in the NMMI. a) Composite red and green fluorescent image after initial seeding. Red circles are used to mark initial locations of the sender organisms. Initially, no green fluorescent cells are observed since AHL has not been received by receiver organisms. b) Composite red and green fluorescent image after ~16 hours of cell culture. AHL has diffused from the sender organisms to activate GFP expression in receiver organisms, while the sender and receiver cells remain physically segregated in nearly all chambers. c) A magnified composite image of red and green fluorescent images shows segregated sender and receiver organisms. d) In this composite red and green fluorescence image, green fluorescence indicates an abundance of receiver cells. The lack of red fluorescent indicates that AHL must have diffused from outside the field of view (at least 500 μm x 700 μm) to activate GFP expression. This is further demonstration of inter-species chemical communication while maintaining physical segregation.

In the time-lapse video S2, which is 100 times faster than real time, it is shown that green fluorescence is observed subsequent to the growth of red fluorescent cells. This does not necessarily mean that green fluorescent cells (the receiver cells) grow more slowly than the red fluorescent cells (the sender cells). In fact, quorum sensing is population and cell density dependent. At low cell densities, synthesis of quorum sensing molecules is limited, while at high cell densities synthesis of quorum sensing molecules rises. When the level of quorum sensing molecules is sufficiently high, it can be used to regulate various genetic activities. Thus, the red fluorescent sender cells first grow to high population density before AHL is synthesized. At sufficient population density, AHL secreted by the sender cells activates GFP expression in the receiver cells, which can be detected via fluorescence microscopy. The delay in green fluorescence observed in video S2 is representative of the dynamics of quorum sensing.

Split channel videos of bright field, green fluorescent and red fluorescent results are provided in supplementary videos S3.1, S3.2 and S3.3. Correspondence between fluorescent cells and all cells living in the NMMI is confirmed. This method suggests opportunities for future experiments on environmental samples, in which fluorescence may not exist. To assist bright field imaging, we incubate the NMMI in a shaking incubator at 37ºC for 3 hours before moving the NMMI to the microscope. This allows us to initially locate where cells are growing when we are using higher magnification (10x). The epi-fluorescence microscope is constructed with bright field illumination coming from the top while fluorescence illumination comes from below, therefore, the fluorescence images are interfered slightly by the bright field illumination. We lower the intensity of the bright field illumination to minimize the interference.

Conclusions

In conclusion, replica molding of PDMS soft lithography has been used to fabricate HEMA-EDMA based micro-well arrays on transparent glass slides. The morphology and transport properties of both microporous and nanoporous HEMA-EDMA were characterized with HIM and a dual chamber diffusion cell, respectively. The resulting Nanoporous Microscale Microbial Incubators (NMMIs) facilitate co-culture of multiple species in chemical communication while remaining physically isolated. This principle was demonstrated by co-culture of an engineered *E. coli* quorum sensing (QS) pair. Results demonstrate that the NMMI co-culture platform is capable of physically isolating bacteria while retaining inter-species chemical communication. The NMMI platform enables high throughput cell culture and real-time observation of growth dynamics.

In the future, the NMMI can be used as a platform to study both competitive and collaborative inter-species communication[34], such as syntrophy [35] and other microbial interactions [36-37]. The NMMI differs from the completely isolated PDMS microwell arrays, which are limited to interrogation of single species phenotypes [38]. It is hypothesized that the NMMI device can also be used to cultivate and isolate uncultivated microbial species. Some believe that many microbes elude laboratory cultivation because they rely upon interactions with other organisms [36], the NMMI could help to identify these organisms. Further, the NMMI can be used to optimize microbial communities for applications in metabolic engineering [39] and synthetic biology [40] that require multiple species.

Acknowledgements

This work was supported by the National Science Foundation under award 1048133.

Notes and references

Electronic Supplementary Information (ESI) available: See DOI: 10.1039/b000000x/

[1] N. R. Pace, *Science*, 1997, **276**, pp. 734–740.
[2] R. I. Amann, W. Ludwig, and K. H. Schleifer, *Microbiol. Rev.*, 1995, **59**, 143–169.
[3] T. P. Curtis, W. T. Sloan, and J. W. Scannell, *Proc. Natl. Acad. Sci.*, 2002, **99**, 10494–10499.
[4] B. J. Tindall, P. Kampfer, J. P. Euzeby, and A. Oren, *Int. J. Syst. Evol. Microbiol.*, 2006, **56**, 2715–2720.
[5] J. T. Staley and A. Konopka, *Annu. Rev. Microbiol.*, 1985, **39**, 321–346.
[6] P. H. Janssen, P. S. Yates, B. E. Grinton, P. M. Taylor, and M. Sait, *Appl. Environ. Microbiol.*, 2002, **68**, 2391–2396.
[7] K. J. Nye, D. Fallon, B. Gee, S. Messer, R. E. Warren, and N. Andrews, 1999, *J. Med. Microbiol.*, **48**, 1111–1114.
[8] S. R. Vartoukian, R. M. Palmer, and W. G. Wade, *Environ. Microbiol.*, 2010, **12**, 916–928.
[9] S. A. Connon and S. J. Giovannoni, *Appl. Environ. Microbiol.*, 2002, **68**, 3878–3885.
[10] J. Song, H.-M. Oh, and J.-C. Cho, *FEMS Microbiol. Lett.*, 2009, **295**, 141–147.
[11] B. C. Ferrari, S. J. Binnerup, and M. Gillings, *Appl. Environ. Microbiol.*, 2005, **71**, 8714–8720.

[12] M. V. Sizova, T. Hohmann, A. Hazen, B. J. Paster, S. R. Halem, C. M. Murphy, N. S. Panikov, and S. S. Epstein, *Appl. Environ. Microbiol.*, 2012, **78**, 194–203.
[13] Y. Aoi, T. Kinoshita, T. Hata, H. Ohta, H. Obokata, and S. Tsuneda, *Appl. Environ. Microbiol.*, 2009, **75**, 3826–3833.
[14] J. Park, A. Kerner, M. A. Burns, and X. N. Lin, *PLoS ONE*, 2011, **6**, e17019.
[15] A. Grodrian, J. Metze, T. Henkel, K. Martin, M. Roth, and J. M. Köhler, *Biosens. Bioelectron.*, 2004, **19**, 1421–1428.
[16] J. R. Moffitt, J. B. Lee, and P. Cluzel, *Lab. Chip*, 2012, **12**, 1487–1494.
[17] A. Groisman, C. Lobo, H. Cho, J. K. Campbell, Y. S. Dufour, A. M. Stevens, and A. Levchenko, *Nat. Methods*, 2005, **2**, 685–689.
[18] E. J. Stewart, *J. Bacteriol.*, 2012, **194**, 4151–4160.
[19] J. F. Edd, D. D. Carlo, K. J. Humphry, S. Köster, D. Irimia, D. A. Weitz, and M. Toner, *Lab. Chip*, 2008, **8**, 1262–1264.
[20] T. Kaeberlein, K. Lewis, S.S. Epstein, *Science*, 2002, **296**, 1127–1129.
[21] D. Nichols, N. Cahoon, E. M. Trakhtenberg, L. Pham, A. Mehta, A. Belanger, T. Kanigan, K. Lewis, and S. S. Epstein, *Appl. Environ. Microbiol.*, 2010, **76**, 2445–2450.
[22] H. J. Kim, J. Q. Boedicker, J. W. Choi, and R. F. Ismagilov, *Proc. Natl. Acad. Sci.*, 2008, **105**, 18188–18193.
[23] L. L. Ling, T. Schneider, A. J. Peoples, A. L. Spoering, I. Engels, B. P. Conlon, A. Mueller, T. F. Schäberle, D. E. Hughes, S. Epstein, M. Jones, L. Lazarides, V. A. Steadman, D. R. Cohen, C. R. Felix, K. A. Fetterman, W. P. Millett, A. G. Nitti, A. M. Zullo, C. Chen, and K. Lewis, *Nature*, 2015, **517**, 455–459.
[24] K. Zengler, G. Toledo, M. Rappé, J. Elkins, E. J. Mathur, J. M. Short, and M. Keller, *Proc. Natl. Acad. Sci.*, 2002, **99**, 15681–15686.
[25] Y. Cheng, C.-Y. Tsao, H.-C. Wu, X. Luo, J. L. Terrell, J. Betz, G. F. Payne, W. E. Bentley, and G. W. Rubloff, *Adv. Funct. Mater.*, 2012, **22**, 519–528.
[26] C. J. Ingham, A. Sprenkels, J. Bomer, D. Molenaar, A. van den Berg, J. E. T. van H. Vlieg, and W. M. de Vos, *Proc. Natl. Acad. Sci.*, 2007, **104**, 18217–18222.
[27] L. Ma, J. Kim, R. Hatzenpichler, M. A. Karymov, N. Hubert, I. M. Hanan, E. B. Chang, and R. F. Ismagilov, *Proc. Natl. Acad. Sci.*, 2014, **111**, 9768–9773.
[28] W. Du, L. Li, K. P. Nichols, and R. F. Ismagilov, *Lab. Chip*, 2009, **9**, 2286–2292.
[29] Y. Xia and G. M. Whitesides, *Annu. Rev. Mater. Sci.*, 1998, **28**, 153–184.
[30] F. L. Geyer, E. Ueda, U. Liebel, N. Grau, and P. A. Levkin, *Angew. Chem. Int. Ed.*, 2011, **50**, 8424–8427.
[31] K. Engberg and C. W. Frank, *Biomed. Mater.*, 2011, **6**, 055006.
[32] R. Weiss and T. F. Knight Jr, *DNA Computing*, A. Condon and G. Rozenberg, Eds. Springer Berlin Heidelberg, 2001, 1–16.
[33] P. D. Straight and R. Kolter, *Annu. Rev. Microbiol.*, 2009, **63**, 99–118.
[34] A. K. Wessel, L. Hmelo, M. R. Parsek, and M. Whiteley, *Nat. Rev. Microbiol.*, 2013, **11**, 337–348.
[35] M. T. Mee, J. J. Collins, G. M. Church, and H. H. Wang, *Proc. Natl. Acad. Sci.*, 2014, **111**, E2149–E2156.
[36] K. Faust and J. Raes, *Nat. Rev. Microbiol.*, 2012, **10**, 538–550.
[37] B. Dura, S. K. Dougan, M. Barisa, M. M. Hoehl, C. T. Lo, H. L. Ploegh, and J. Voldman, *Nat. Commun.*, 2015, **6**.
[38] E. M. Bradshaw, S. C. Kent, V. Tripuraneni, T. Orban, H. L. Ploegh, D. A. Hafler, and J. C. Love, *Clin. Immunol. Orlando Fla*, 2008, **129**, 10–18.
[39] S. K. Lee, H. Chou, T. S. Ham, T. S. Lee, and J. D. Keasling, *Curr. Opin. Biotechnol.*, 2008, **19**, 556–563.
[40] K. Brenner, L. You, and F. H. Arnold, *Trends Biotechnol.*, 2008, **26**, 483–489.
[41] S. T. Flickinger, M. F. Copeland, E. M. Downes, A. T. Braasch, H. H. Tuson, Y.-J. Eun, and D. B. Weibel, Journal of the American Chemical Society, 2011, 133, 5966–5975.
[42] B. P. Casavant, E. Berthier, A. B. Theberge, J. Berthier, S. I. Montanez-Sauri, L. L. Bischel, K. Brakke, C. J. Hedman, W. Bushman, N. P. Keller, and D. J. Beebe, "Suspended microfluidics," Proceedings of the National Academy of Sciences, vol. 110, no. 25, pp. 10111–10116, Jun. 2013.
[43] R. Menon and K. S. Korolev, "Public Good Diffusion Limits Microbial Mutualism," Physical Review Letters, vol. 114, no. 16, Apr. 2015.

